AIAA 98-4189

Effect of Unbalanced Attitude Control Burns on STARDUST Trajectory Design

E. Hirst and C. Yen

Jet Propulsion Laboratory
California Institute of Technology
Pasadena, California

AIAA/AAS Astrodynamics Specialist Conference
August 10-12, 1998 / Boston, MA

EFFECT OF UNBALANCED ATTITUDE CONTROL BURNS ON STARDUST TRAJECTORY DESIGN*

Edward A. Hirst†, Chen-wan L. Yen†,
Jet Propulsion Laboratory, California Institute of Technology
4800 Oak Grove Drive, Pasadena, California 91109

Abstract

STARDUST (Discovery IV) is a comet, Wild-2, flyby sample return mission. Sample contamination concerns have resulted in a spacecraft design with an unbalanced thruster configuration that imparts translational forces during all attitude control (ACS) activities. Due to the long duration of the mission (7 years), it is desirable to determine the cumulative nature of these unbalanced ACS forces and their effect on the mission's delta-V (ΔV) budget. In addition, high precision Earth re-entry and comet delivery requirements require determining the effect of these unbalanced ACS forces on the ability to achieve the required navigation delivery accuracies. This paper describes the STARDUST spacecraft ACS modes, mechanisms, history, and corresponding mathematical models. Integration of these models into a standard Jet Propulsion Laboratory (JPL) trajectory propagator and optimizer allows trajectory design studies to characterize the effect of the ACS perturbations. It is shown that 1) ACS activities impart a cumulative impulse amounting to 16 m/s, 2) the ΔV budget for the mission could increase by as much as 43 m/s, post-launch, if modeling of ACS activity were not performed, and 3) the ACS perturbation contribution to navigation delivery errors are insignificant compared to expected navigation errors at comet encounter, but must be accounted for during Earth return.

---

* The study described in this paper was performed by the Jet Propulsion Laboratory, California Institute of Technology, under contract with the National Aeronautics and Space Administration.

† Member of Technical Staff, Mission and Systems Architecture Section

Introduction

STARDUST is the fourth mission of NASA's Discovery program. Its primary science goal is to collect comet Wild-2 coma dust samples in an aerogel medium and return them to Earth. Bonus science is anticipated in the form of collection of interstellar particles (ISP), images of the comet coma and nucleus, and in-situ comet and dust particle analysis and flux monitoring[1]. Figure 1 illustrates the spacecraft trajectory for the first launch opportunity.

The STARDUST spacecraft is shown in Figure 2 in its encounter configuration. The aerogel medium, when in use, is deployed above the spacecraft upper deck (+z-axis). The spacecraft is three-axis stabilized using active thruster control. To avoid contamination of the aerogel medium, all of the thrusters are mounted on the lower deck (-z-axis). This thruster configuration imparts an unbalanced force, i.e. translational thrust, to the spacecraft every time attitude control burns are executed.

Over the seven-year mission, the cumulative ACS activity is estimated to amount to tens of meters per second. The sum of trajectory correction maneuvers required to compensate for the ACS burns could be intolerably large unless the ACS effects are accounted for in advance while designing the baseline trajectory. Four deterministic Deep Space Maneuvers (DSM) are used to shape the trajectory and 14 statistical maneuvers are planned to navigate the trajectory. The statistical maneuvers support correction of errors in Launch (L) injection, DSM execution, Earth flyby (EGA), Wild-2 flyby (E) and approach to Earth return (R). Table 1 provides a summary of the mission's maneuver profile.

The ACS activity is also expected to affect navigation delivery accuracy, which is especially important during two events: comet encounter and Earth return. The bulk of the encounter sequence of activities transpires very rapidly within a few minutes of closest approach to the comet. Inaccuracies in the delivery of the

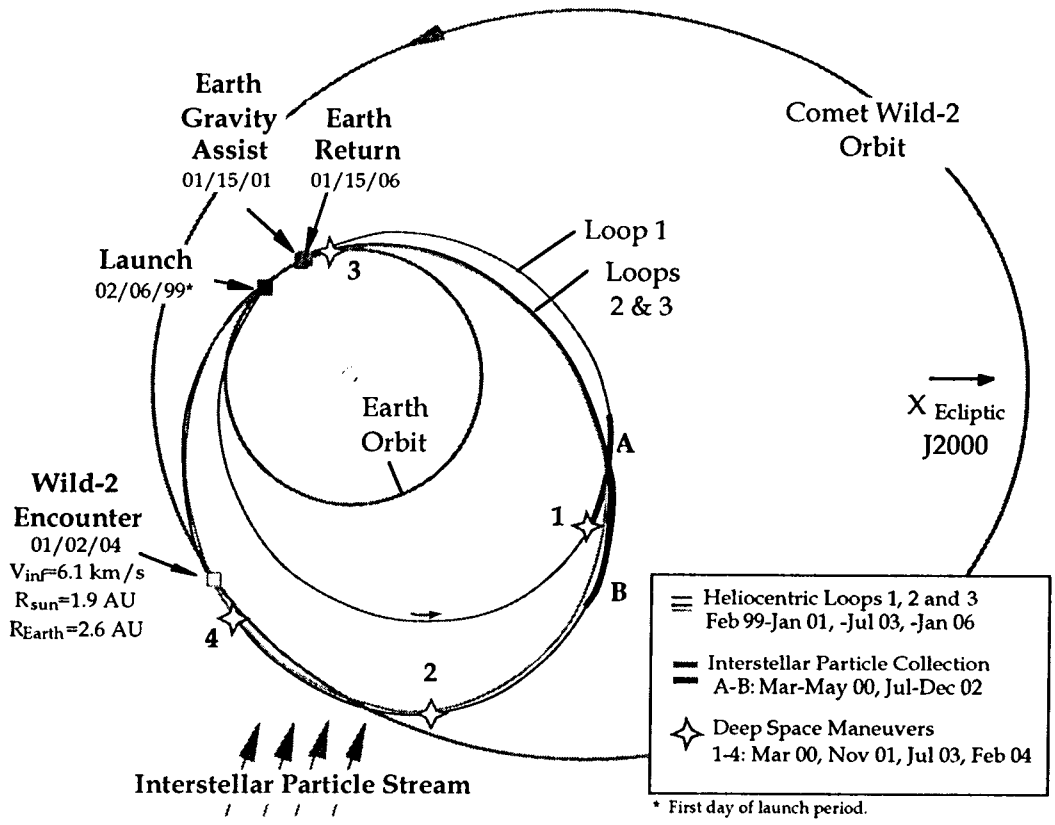

Figure 1. STARDUST Heliocentric Trajectory

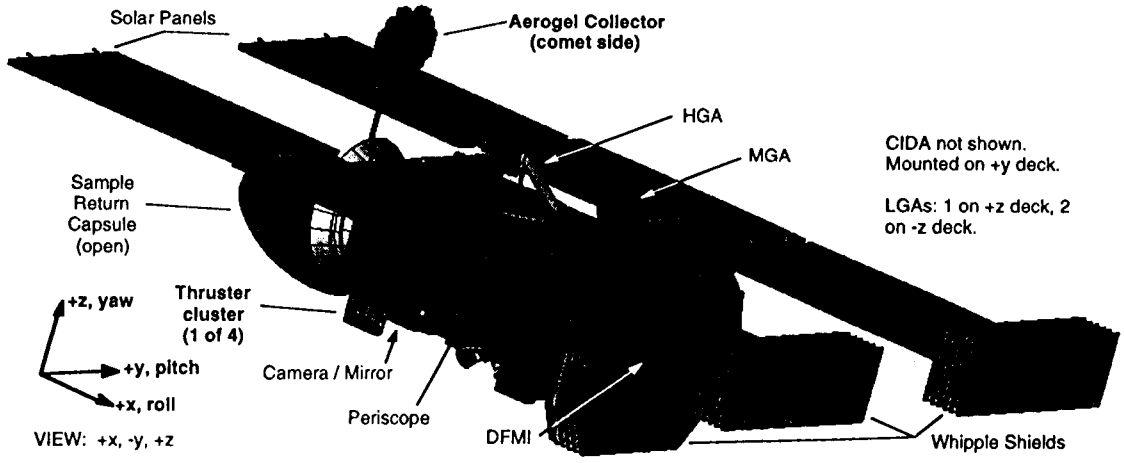

Figure 2. STARDUST Spacecraft[‡]

[‡] Courtesy Lockheed Martin Astronautics

Table 1. Trajectory Correction Maneuver Profile

TCM#	Date	Nature	Comment
1	L+15d	S	Injection correction
2	1st aphelion	D	DSM-1, large
3	DSM+30d	S	DSM clean-up
4	EGA-60d	S	EGA targeting
5	EGA-10d	S	EGA targeting
6	EGA+30d	S	EGA clean-up
7	2nd aph.	D	DSM-2, small
8	2nd perih.	D	DSM-3, large
9	DSM+7d	S	DSM clean-up
10	E-30d	S	Wild-2 targeting
11	E-10d	S	Wild-2 targeting
12	E- 2d	S	Wild-2 targeting
13	E- 6h	S	Wild-2 targeting
14	E+30d	D	DSM-4, small
15	3rd aph.	S	Earth Return targeting
16	R-60d	S	Earth Return targeting
17	R-13d	S	Earth Return targeting
18	R- 1 d	S	Earth Return targeting

where: D = deterministic, S = statistical

spacecraft could preclude achievement of the desired science objectives. Upon return to Earth, a sample return capsule will separate from the spacecraft, directly enter the atmosphere, and land at the Utah Test and Training Range (UTTR). Accurate navigation is again required to meet the entry corridor conditions for successful delivery of the return capsule.

In the sections to follow, we will present two mathematical models used to describe the ACS activity, the ΔV budget and navigation delivery assessment process, and the corresponding results.

Attitude Control Perturbation Models

The ACS perturbation is divided, by source, into two categories: (1) due to almost continuous limit cycling and (2) due to less frequent attitude slewing required for communications, maneuvers and other special activities. Two different models are constructed to handle each case.

It should be noted that the modeling described herein addresses only the deterministic (known) effects of the ACS activity. No attempt is made to account for uncertainties and their implications. These are considered the domain of navigation activities.

Limit Cycle Model

The limit cycle model simulates the behavior of the attitude control system (ACS) resulting from maintaining the spacecraft attitude with the desired angular deadbands.

Spacecraft Attitude Modes The direction of the ACS acceleration is established based on the pre-flight plan for spacecraft attitude. In the limit cycle model, the direction of the ACS force is parallel to the spacecraft +z-axis. The ACS forces in the other two axes cancel out on average.

The limit cycle spacecraft attitude is divided into four main modes. Table 2 describes these modes, and submodes, in terms of spacecraft axis alignment. Table 3 gives three different deadband control values that can be imposed at various phases of the mission. Table 4 provides the spacecraft attitude history as a function of mission elapsed time, in terms of the modes and deadbands given in Tables 2 and 3.

Table 2. Limit Cycle Attitude Modes

Mode	Mode No.	First axis	Second axis
1. Sunpoint			
submode:	11	+z = -r	+y = -r X v
	12	+z = -r	+y = +r X v
2. Constant off-sun angle			
submode:	21, 22	same as above*	
* followed by a single axis rotation about +y axis			
3. Interstellar Particle (ISP) collection			
submode:	31	+z = -r	+y = -r X ivr
	32	+x = ivr	+y = -r X ivr
4. Cometary and Interstellar Dust Analyzer (CIDA) experiment			
submode:	41	+x = -ivr	+y = -r X ivr
	42*	+z = -r	+y = -r X ivr
* followed by a single axis rotation about +y axis			

where:

+x, +y, +z	= unit spacecraft x, y, z axis vectors
r, v	= unit spacecraft position and velocity
ivr	= unit interstellar particle velocity vector relative to spacecraft

Table 3. Limit Cycle Deadbands

Mode	Deadband	Comments
1	x,y,z = 15°	Used during bulk of Cruise
2	x,y = 2°, z = 10°	Near Encounter
3	x, y, z = 10°	Cruise option 2

Attitude Control Force Modeling The magnitude of the acceleration imparted by the ACS system is determined by calculating the average thruster activity or pulse frequency. This frequency is equivalent to the number of times the spacecraft's angular motion results in deadband violation. The average pulse frequency can be quantified as a function of spacecraft mass distribution, ACS thruster characteristics and configuration, mission geometry, and expected solar torques. Pulse frequencies can then be converted to average perturbative accelerations for easier consideration during trajectory design.

Table 4. Limit Cycle Attitude Schedule

Days From Launch	Attitude Mode	Attitude Submode	Off-sun Angle (deg)	Deadband Mode
0	Off-sun	21	45	1
30	Off-sun	22	22	1
45	CIDA	41	-	1
54	CIDA	42	20	1
144	Sunpoint	11	-	1
369	Sunpoint	12	-	1
403	ISP	31	-	1
453	ISP	32	-	1
469	Sunpoint	12	-	1
668	Sunpoint	11	-	1
704	Off-sun	21	17	1
709	Off-sun	21	45	1
728	Off-sun	22	20	1
744	Sunpoint	12	-	1
769	CIDA	41	-	1
780	CIDA	42	20	1
914	Sunpoint	11	-	1
1053	Sunpoint	12	-	1
1065	Sunpoint	12	-	3
1267	ISP	31	-	1
1385	ISP	32	-	1
1402	Sunpoint	11	-	1
1523	Sunpoint	12	-	1
1658	Sunpoint	11	-	1
1703	CIDA	42	20	1
1747	Off-sun	22	3	1
1760	Off-sun	22	5	1
1770	Off-sun	22	7	1
1780	Off-sun	22	16	1
1790	Off-sun	22	18	2
1805	Off-sun	22	20	1
1811	Sunpoint	12	-	1
1965	Sunpoint	11	-	1
2000	Sunpoint	11	-	3
2165	Sunpoint	11	-	1
2185	Sunpoint	12	-	1
2456	Sunpoint	11	-	1
2489	Off-sun	21	21	1
2509	Off-sun	22	45	1
2534	Off-sun	22	26	1

Spacecraft thruster performance (thrust magnitude) is modeled according to the manufacturer's specifications. Accurate modeling of this system is necessary because the performance differs appreciably across the duration of the mission.

A semi-empirical model of ACS force was developed at Lockheed-Martin Astronautics and follows the steps and equations given below[2].

The thrust level of the ACS thrusters depends on the feed pressure of the blow-down propulsion system, which is given by the following equation.

$$p = \frac{p_o u_o}{\left[u_o + \frac{m_o - m}{mp_o(1-u_o)} \right]} \quad (1)$$

where:

p_o = initial tank pressure (psi)

u_o = initial tank ullage (mp_o / m_o)

m_o = initial total spacecraft mass (kg)

mp_o = initial propellant mass (kg)

m = current spacecraft mass (kg)

p = current tank pressure (psi)

The thrust magnitude per pulse (f_{bit}) is then obtained from the following derived equation. The factor of 2 indicates that a thruster pair is fired when a deadband limit is tripped.

$$f_{bit} = 2*(0.0067 + 0.00004984p) \text{ (N)} \quad (2)$$

Rigid body dynamics is invoked to calculate the thruster pulse frequency required to maintain spacecraft motion within the desired attitude deadbands. The following are used to calculate the thruster firing frequency for each of the spacecraft axis.

$$n_x = \frac{\tau_{sx} \cos^2\theta_s (R_{max} - R) R_{min}^2}{l_x f_{bit} (R_{max} - R_{min}) R^2} + \frac{l_x f_{bit} (R - R_{min})}{4 db_x I_{xx} (R_{max} - R_{min})} \quad (3)$$

$$n_y = \frac{\tau_{sy} \cos^2\theta_s R_{min}^2}{l_y f_{bit} R^2} \quad (4)$$

$$n_z = \frac{l_z f_{bit}}{4 db_z I_{zz}} \quad (5)$$

$$n_T = n_x + n_y + n_z \quad (6)$$

where:

n_* = thruster pulse frequency (1/s) per axis

τ_{s*} = solar torque (x-, y-axis) (Nm)

θ_s = z-axis off-sun angle, attitude dependent

R_{***} = solar range (max, min, current) (AU)

l_* = effective thruster moment arms (m)

I_{**} = mass moments of inertia (kgm^2)

db_* = deadband limits (radians)

Notice that the equations decouple the motion in each spacecraft axis to facilitate the modeling process. The motion about the y-axis of the spacecraft is driven primarily by the influence of the solar torque. On the other hand, the solar torque component in the spacecraft z-axis is relatively small and ignored. The degree to which motion about the x-axis is influenced by solar torque is determined by the solar range history of the mission. Near the sun (R≈Rmin),

solar torque is the driving force behind the motion. Far from the sun (R≈Rmax), the influence of solar torque is minimal and the motion is steady state or pure limit cycling.

The thruster pulse frequencies are then combined with the minimum impulse bit and attitude information to produce an average ACS force and corresponding acceleration. An average mass flow rate is also calculated to keep track of the change in the mass of the spacecraft due to the ACS activity. These values are calculated via the following equations.

$$\vec{f} = f_{bit} n_T \vec{k} \tag{7}$$

$$\vec{a} = \vec{f} / m \tag{8}$$

$$\dot{m} = \frac{f_{bit} n_T}{Isp_{acs} g} \tag{9}$$

where:

$\vec{f}$ = ACS force vector (m/s)
$\vec{k}$ = unit vector in the direction of +z axis
$\vec{a}$ = ACS acceleration vector (m/s^2)
$\dot{m}$ = mass flow rate (kg/s)
Isp_{acs} = ACS thruster specific impulse (s)
g = gravity at Earth's surface (m/s^2)

The ACS force model parameters used in this paper are summarized in Table 5. Deterministic mass decrements due to deterministic maneuvers were also included in the modeling runs.

Table 5. ACS Force Parameters

Parameter	Value	Parameter	Value
Po	281 psi	Ix	0.110 m
Uo	0.35	Iy	0.455 m
Mo	398 kg	Iz	0.125 m
Mpo	85 kg	Ixx	88 kgm^2
τ sx	1.7E-7 Nm	Iyy	200 kgm^2
τ sy	1.6E-5 Nm	Izz	272 kgm^2
Rmax	2.7 AU	Isp-acs	100 s
Rmax	1.0 AU	g	9.807 m/s^2

Limit Cycle ACS Perturbation Profile

The profile of resulting thruster pulse frequency, mass flow rate, acceleration and acceleration direction as a function of mission time are illustrated in Figures 3 - 6.

Notice that the histories share the same basic shape. This shape is driven primarily by the dependence of the modeling on the solar range history of the mission. Peak ACS activity occurs at minimum solar range when the solar torques are the strongest.

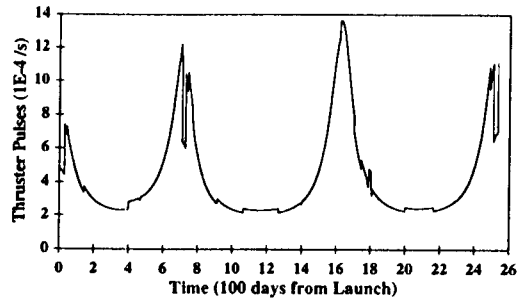

Figure 3. Total Thruster Pulse History

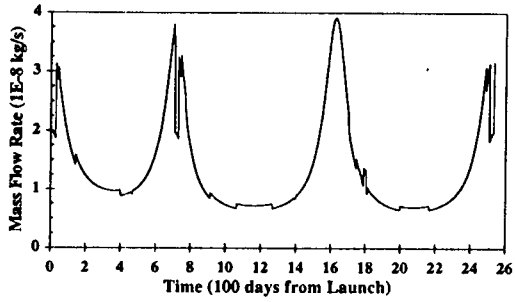

Figure 4. Mass Flow Rate History

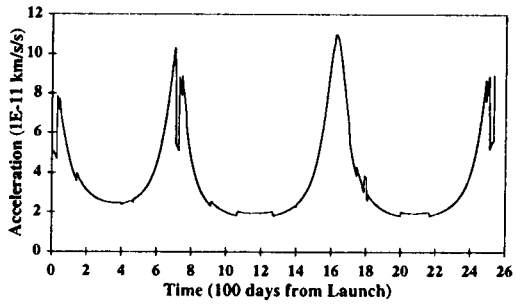

Figure 5. Acceleration Magnitude History

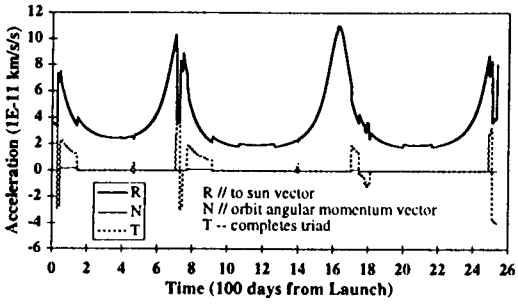

Figure 6. Acceleration Components

The discontinuities in these profiles are the result of one of three events in the mission's attitude profile. Most notable are planned changes in the z-axis off-sun angle. These are most visible when the spacecraft is near Earth

(launch, EGA, return). Large off-sun angles are required during these periods to meet simultaneous power and communications requirements. Other occurrences are due to off-sun pointing in support of interstellar particle cruise science.

More subtle variations can be seen when limit cycle deadbands are changed or when deterministic mass decrements are scheduled. The deadband variations are most visible near second and third aphelion. The largest mass decrement occurs at the first deterministic maneuver (near Launch+400 days).

Finally, in Figure 6, notice that the direction of the ACS perturbation is consistent with the ACS thrust being directed toward the -z-axis of the spacecraft. Tangential perturbations (T-direction) occur primarily during off-sun pointing near Earth and during cruise science.

Slew Model

The second source of ACS perturbations is spacecraft slewing (relatively quick turns) to support communications, optical navigation (opnav) and transitions between different attitude phases of the mission. Slews associated with trajectory correction maneuvers are ignored and assumed to be accounted for in the design of the maneuvers.

The modeling of these slews is built on predetermined goals and operational rules. The detailed equations have been developed by Lockheed-Martin Astronautics[3].

Slew Elements, Events and Equations

Slew activity on STARDUST need only account for spacecraft turns about two axes: the y-axis and the z-axis. A turn about the y-axis is designated as a pitch slew, and turn about the z-axis as a yaw slew. Roll, a turn about the spacecraft x-axis, completes the triad, but is not anticipated very frequently during the mission and as such is not a key component of the modeling. Figure 1 further illustrates these turn angles.

A spacecraft slew event (group of turns) is comprised of a sequence of slew elements (single turn). Table 6 shows eight different slew elements, divided by turn axis and magnitude. Each element produces a corresponding perturbing ΔV and mass decrement. Spacecraft slewing has been limited to these slew elements to reduce complexity during mission operations. The ΔV (x,y,z) reference used in Table 6 is a coordinate frame that is fixed in inertial space and coincident with the spacecraft body frame at the initiation of each slew.

Table 6. Slew Elements and ΔV Equations

Element	Description	ΔV (m/s), Δm (g)
1	To event attitude* pitch Size: 0°-15°	$\Delta Vx = 1.4217*\sin(P)/m$ $\Delta Vy = 0$ $\Delta Vz = 1.4217*(1+\cos(P))/m$ $\Delta m = 3.0$
2	To event attitude* pitch Size: 15°-45°	$\Delta Vx = 1.7060*\sin(P)/m$ $\Delta Vy = 0$ $\Delta Vz = 1.7060*(1+\cos(P))/m$ $\Delta m = 3.6$
3	To event attitude* pitch/yaw Size: 0°-30°	$\Delta Vx = 2.6540*\sin(P)/m$ $\Delta Vy = 0$ $\Delta Vz = 2.6540*(1+\cos(P))/m$ $\Delta m = 5.6$
4	Deadband clamp	$\Delta Vx = 0, \Delta Vy = 0$ $\Delta Vz = 2.4629/m$ $\Delta m = 2.6$
5	From event attitude** pitch Size: 0°-15°	$\Delta Vx = 0.1442*\sin(P)/m$ $\Delta Vy = 0$ $\Delta Vz = 0.1442*(1+\cos(P))/m$ $\Delta m = 0.3$
6	From event attitude** pitch Size: 15°-45°	$\Delta Vx = 0.4264*\sin(P)/m$ $\Delta Vy = 0$ $\Delta Vz = 0.4264*(1+\cos(P))/m$ $\Delta m = 0.9$
7	From event attitude** pitch/yaw Size: 0°-30°	$\Delta Vx = 0.8052*\sin(P)/m$ $\Delta Vy = 0$ $\Delta Vz = 0.8052*(1+\cos(P))/m$ $\Delta m = 1.7$
8	Yaw only** Size: 30°-180°	$\Delta Vx = 0, \Delta Vy = 0$ $\Delta Vz = 2.085/m$ $\Delta m = 2.2$

where: P = pitch angle, m = spacecraft mass
* = includes deadband tightening
** = no deadband tightening required

Pure pitch slews (elements 1-2, 5-6) are typically performed to and from a sun pointed +z-axis orientation which is the most common background attitude orientation of the mission. Compatibly, pure yaw slews (element 8) are performed only when the spacecraft is in a sun pointed +z-axis orientation. Occasionally, both pitch and yaw turns are required during a slew event. When yaw angles are small (<30 degrees) the spacecraft turns are combined and performed simultaneously (elements 3 and 7). However, when yaw angles are large (>30 deg), the slew event is constructed of a sequence of slew elements, typically pitch-yaw-pitch or a subset thereof.

Review of all slew events occurring during the mission reveals that one of seven slew event modes, described in Table 7, can accomplish the attitude change objectives associated with any slew event. In Table 7 (column 3), "To" entries list the slew elements

that are required to change the attitude from the cruise or background state to the attitude required for the event. "From" entries, correspondingly, list the slew elements required to return the spacecraft to the cruise or background attitude. Attitude phase slew events, however, are a change in the cruise or background attitude. They are one-way in nature and use the "From" sequence entries only.

Table 7. Slew Event Modes

Mode	Description (usage)	Slew sequence
1	deadband clamp only (comm)	To: 4 From: -
2	pitch only (mode change, comm)	To: 1 / 2 From: 5 / 6
3	pitch, yaw, pitch (mode change, comm)	To: 5 / 6, 8, 1 / 2 From: 5 / 6, 8, 5 / 6
4	pitch/yaw combined (mode chg, opnav, comm)	To: 3 From: 7
5	yaw only (mode change)	To: 8, 4 From: 8
6*	pitch, yaw (mode change)	To: 5 / 6, 8, 4 From: 5 / 6, 8
7*	yaw, pitch (mode change, comm)	To: 8, 1 / 2 From: 8, 5 / 6

* For round trip mode 6 or 7 slew, index is switched from 6 to 7, or 7 to 6, as appropriate, after 'To' slews.

One ΔV vector is produced for each slew event. The series of slew elements for each slew event is collapsed to a single event time and single ΔV. The resulting ΔV contains ΔV's accumulated during the turn to the event attitude, the turn from the event attitude and the time spent limit cycling at the event attitude. The last of these is important because the event deadbands are typically smaller than the background limit cycle deadbands. In order to not double book keep ACS perturbations, it is necessary to subtract the ΔV contributions from the limit cycle model.

Spacecraft Attitude and Slew History

The baseline spacecraft attitude profile is needed to match scheduled slew events with slew event modes as a function of turn magnitudes and turn characteristics. The burden of selecting the appropriate slew event mode is placed on the analyst, but this approach is selected in favor of the extensive coding that would be required to make the slew event mode selection completely autonomous.

The formulation of attitude modes is slightly modified for the calculation of slew ΔV's as compared to the limit cycle model. The new formulation is referenced to a Sun-Earth-Spacecraft plane, consistent with current ACS flight software, and not the orbit plane as used in limit cycle modeling. Limit cycle modeling for trajectory optimization is referenced to the orbit plane in order to not introduce the Earth ephemeris into the optimization problem. The small error introduced by this split attitude description approach is deemed acceptable.

The new attitude formulation is comprised of a different, but fairly equivalent, set of attitude modes. The formulation is expanded to include communications and opnav specific modes. Table 8 summarizes the attitude modes available in this new formulation. Table 9 provides five different deadband modes, also expanded from the limit cycle set to include opnavs and communications.

Table 8. Slew Attitude Modes

Mode	First axis	Second axis
1. Constant off-sun	**kk** = rotate **rr**, angz, about **nn**	**jj** = ±**kk** X **tt**, if angy = 0, 180
2. CIDA tracking	**ii** = **ivr**	**jj** = **rr** X **ivr**
3. CIDA off-sun	**kk** = rotate **rr**, angz, about **n-isp**	**jj** = **kk** X **ivr**
4. Earth tracking	**kk** = **re**	**jj** = **rr** X **kk**
5. ISP collector	**kk** = **rr**	**jj** = **ivr** X **kk**
6. ISP tracking	**ii** = -**ivr**	**jj** = **rr** X **ii**
7. DSMs	- not used	
8. Opnav during option #3	**kk** = rotate **rr**, angf, about **n-isp**	**jj** = **xim** X **kk**
9. Opnav during option #12	**kk** = same as 12	**jj** = **kk** X **xim**
10. Encounter*	**ii** = **uws**	**jj** = **re** X **ii**
11. Medium Gain Antenna comm	**kk** = rotate **rr**, angl, about **nn**	**jj** = ±**rr** X **kk**, if angl ≥0, <0
12. High Gain Antenna comm	**kk** = **re**	**jj** = ±**rr** X **kk**, if opt = 0,1
13. Opnav during option #11	**kk** = same as 11	**jj** = **kk** X **xim**
14. Opnav during option #10	**kk** = same as 10	**jj** = **kk** X **xim**

where:

ii, jj, kk	= spacecraft x, y, z axis unit vectors
rr, nn, tt	= reference SPE plane attitude, **rr** = to sun, **nn** = ±**re** X **rr** (**nn**(3)>0), **tt** = **nn** X **rr**
angz	= angle between **kk** and **rr**, positive about **nn**
angy	= angle between **jj** and **nn**, positive about **rr**
n-isp	= isp plane normal, **n-isp** = **ivr** X **rr**
re	= to Earth vector
ivr	= isp to s/c relative velocity
xim	= to image vector
uws	= unit comet to s/c relative velocity
angf	= off-sun angle for CIDA3
angl	= angle between **rr** and **re**, minus mgaoff
mgaoff	= mga off +z boresight angle
opt	= input flag that allows the +y axis to be flipped during HGA comm.
*	= vectors evaluated at closest approach

Table 9. Slew Deadbands

Mode	Deadband	Comments
1	x,y,z = 15°	Cruise option 1
2	x, y, z = 10°	Cruise option 2
3	x,y = 2°, z = 10°	HGA / Near encounter
4	x, y, z = 6°	MGA comm
5	x, y, z = 0.25°	Image

Table 10 contains the mission slew requirement profile that is consistent with the new formulation. It also contains the slew mode schedule for transitions between attitude phases. There are 39 different attitude phases planned during the mission, but nine transitions occur naturally and do not require any spacecraft slewing.

Table 10. Slew and Attitude Profile

Start (dFL)	Atti. Mode	Angz (deg)	Angy (deg)	dead band	Slew Mode
0	1	-45	180	1	0
30	1	22	0	1	3
45	2	-	-	1	3
54	3	-20	-	1	0
144	1	0	180	1	4
369	1	0	0	1	5
403	5	-	-	1	5
453	6	-	-	1	0
469	1	0	0	1	6
668	1	0	180	1	5
704	1	-17	180	1	2
709	1	-45	180	1	2
728	1	20	0	1	3
744	1	0	0	1	2
769	2	-	-	1	7
780	3	-20	-	1	0
914	1	0	180	1	4
1053	1	0	0	1	5
1065	1	0	0	2	0
1267	5	-	-	1	5
1385	6	-	-	1	0
1402	1	0	180	1	4
1523	1	0	0	1	5
1658	1	0	180	1	5
1703	3	-20	-	1	7
1747	11	-	-	1	3
1780	12	-	-	1	2
1789	10	-	-	3	4
1792	12	-	-	3	4
1805	12	-	-	1	0
1811	1	0	0	1	2
1965	1	0	180	1	5
2000	1	0	180	2	0
2165	1	0	180	1	0
2185	1	0	0	1	5
2459	1	0	180	1	5
2489	1	-21	180	1	2
2509	1	45	0	1	3
2533	1	26	0	1	2

where: dFL = days from launch

Slews for communications comprise the bulk of slewing activity with 630 events. The communications schedule only includes those communications events that require a slew or deadband clamp. This results in no slews scheduled just after launch, at and just after EGA, at and just after encounter, and just prior to Earth return. Communications during the near-Earth phases are handled via the low-gain antennas which have very large fields of view. At encounter, by design, the Earth finds itself aligned with the high-gain antenna boresight and no slew is required. Communication periods are typically 4 hours in duration. Shorter periods, 3 hours, are scheduled near aphelion to address power concerns, and longer periods, 8 to 24 hours are scheduled during important mission events (EGA, encounter). Tables 11 and 12 summarize the communications schedule and corresponding slew event modes.

Table 11. High-Gain* Communications

Time (dFL) : # contacts	Slew Mode	Time (dFL) : # contacts	Slew Mode
261-402 : 5	2	1705-1712 : 2	3
403-432 : 19	4	1719-1746 : 6	4
464 : 1	3	1749-1777 : 8	2
499 : 1	2	1780-1810 : 14	1
940-1220 : 9	2	1843-1878 : 2	2
1339-1374 : 2	4	2065-2340 : 9	2
1409-1616 : 7	2		

* attitude mode = 12

Table 12. Medium-Gain* Communications

Time (dFL) : # contacts	Slew Mode	Time (dFL) : # contacts)	Slew Mode
32-44 : 5	2	807-912 : 16	2
51-79 : 5	3	919-1262 : 57	2
86-142 : 9	4	1269-1283 : 3	7
149-401 : 49	2	1290-1395 : 14	4
433-451 : 11	7	1402-1696 : 73	2
454-457 : 2	3	1747-1779 : 24	1
471-765 : 114	2	1811-2508 : 156	2
772-800 : 5	3		

* attitude mode = 11

The opnav schedule is defined in terms of an image vector to which the navigation camera field of view must be oriented. A one-axis moveable mirror allows the camera field of view to rotate about the y-axis of the spacecraft in a plane parallel to the spacecraft x-z plane. This spacecraft capability allows imaging to be compatible with several other attitude modes. This compatibility is reflected in Table 8 and the creation of attitude modes 8, 9, 13 and 14. All opnav slews are modeled through the combined pitch/yaw slew mode (#4). Table 13 summarizes the opnav schedule in terms of time from encounter, opnav frequency, and image vector.

Slew ACS Perturbation Profile The profile of resulting ΔV magnitudes and directions are illustrated in Figures 7-9.

Table 13. Opnav Schedule

Time (E+days)	opnav rate	# of opnavs	Image RA(deg)	Image DEC(deg)
-90 to -50	1 /wk	6	4.86-5.56	165.41-161.18
-50 to -7	2 /wk	12	5.56-5.85	161.16-159.77
-7 to -2	1 /day	5	5.85	159.77
-2 to -1	1 /3hrs	8	5.85	159.77
-1 to -0.5	1 /hr	13	5.85	159.77

where: E = Encounter
Image directions in EME J200

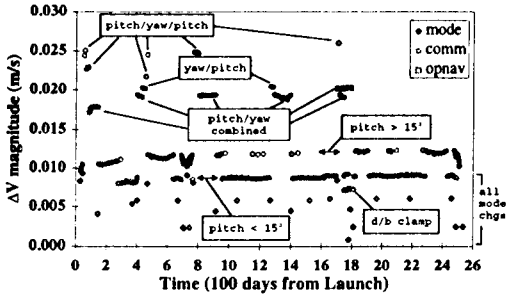

Figure 7. Slew ΔV Magnitude Profile

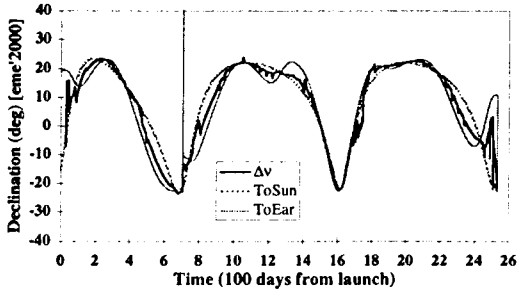

Figure 8. Slew ΔV Declination

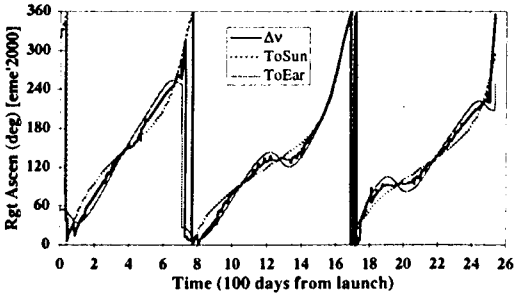

Figure 9. Slew ΔV Right Ascension

Minimum ΔV's occur during pitch-only one-way slews associated with attitude phase transitions. Most ΔV's hover at about 0.008 m/s per event and correspond to pitch-only communications events. Maximum ΔV's correspond to slew modes involving a yaw slew, which can be traced to the inefficiency of the thruster configuration in producing moments about the spacecraft z-axis. The thrusters are mounted in the direction of the -z-axis, but are canted to provide off-axis control. The cant angles, however, are moderate (less than 30 degrees)and result in large cosine losses.

The majority of spacecraft slewing is attributed to communications. Communications slew events typically change the spacecraft attitude from a sunpoint, or near sunpoint, attitude to an Earth point, or near-Earth point attitude. This is evident in the ΔV direction profiles as the ΔV direction stays close to the sun and Earth point directions.

ACS Perturbation Assessment

If the ACS perturbations described above are disregarded in the trajectory propagation and optimization process, the resulting trajectory leads to an inaccurate flight path and faulty ΔV allocations for the STARDUST mission. Since the perturbations are small, approximately $1x10^{-5}$ to $3x10^{-5}$ times local solar gravity, it is possible, in principle, to allow the errors to grow and then have them removed at the eighteen scheduled maneuver locations. The questions that can be posed in this process are: 1) how much extra ΔV must be budgeted for post launch corrections to account for ACS activity?, 2) how much ΔV savings can be realized if the trajectory is re-optimized while accounting for ACS activity in the optimization process?, and 3) how does disregarding the ACS activity affect the accuracy of navigation deliveries at comet encounter and Earth return?

Answering these questions is a cumbersome undertaking, as exhibited by the tedious analyses shown in the earlier sections. It required extensive analytical simulations of the spacecraft activities, the attitude history and the ACS burn strategies. To address questions 1 and 2, additional analyses depicting parameter sensitivities (partial derivatives) were required before incorporating the modeling into the larger parametric optimizer code.

Delta-V Budgets To address questions 1 and 2, three different optimized trajectories were generated:

A) Optimal without ACS Model: This case presents a reference trajectory (pre-launch path)

without ACS perturbations. There are four DSMs required in the trajectory.

B) Error Corrections at Maneuvers: This case considers the presence of ACS forces as an error source during post-launch re-propagation of the trajectory. The ACS perturbations introduce state errors that are evaluated at the maneuver locations. At each maneuver location, a retargeted and reoptimized trajectory is computed (without considering ACS perturbations) to remove the errors caused by the presence of ACS pertubations in the previous leg. This results in 18 revised deterministic ΔV maneuvers during the mission.

C) Optimal with ACS Model: This case takes advantage of the ACS perturbation models during trajectory optimization. An optimal trajectory including ACS perturbations is generated, providing the real answer to the questions at hand.

The following mission parameters were assumed in the analysis:

- Launch date: February 6, 1999
- Injection Energy (C_3): 26 km^2/s^2
- DSM locations constrained to prescribed times for operational reasons.
- Four 1.0 lb-f (4.45 N) thrusters with a specific impulse of 220 seconds assumed for finite ΔV burns.
- Two 0.2 lb-f (0.89 N) thrusters with specific impulse of 100 seconds assumed for ACS burns.
- Initial spacecraft mass: 398 kg.

The ΔV and mass consumption (ΔM) profiles for each of these cases is summarized in Tables 14 through 17.

Navigation Deliveries The answer to question 3 can be simple, provided we regard the ACS perturbations as deterministic in nature. In actuality, the ACS perturbations are far from deterministic and estimated to be in error by as much as 30% (3-σ). One can make a very simple estimate of the ACS activity contribution to the navigation delivery errors at Wild-2 and Earth return by assuming that the stochastic components of the ACS perturbations and all other error sources are addressed in the orbit determination and stochastic maneuver errors. The last maneuvers before Wild-2 encounter or Earth return are planned to be executed within one day of delivery. The position (δx) and velocity (δv) error growth can be bounded as follows:

$$\delta x = \tfrac{1}{2} a_{acs} t^2 \qquad \delta v = a_{acs} t \qquad (10)$$

where:

a_{acs} = ACS perturbation (km/s^2)

t = error growth time (s)

Table 14. ΔV, ΔM Profile: Optimal Trajectory without ACS Model (Case A)

TCM	Time dd mmm yy	Time (dFE)	ΔV (km/s)	ΔM (kg)
2	10 Mar 00	-1393	1.613E-01	28.666
7	30 Nov 01	-763	1.310E-03	0.224
8	14 Jul 03	-172	6.536E-02	11.014
14	01 Feb 04	+30	2.357E-07	0.000
		Total:	2.279E-01	39.904

where: dFE = days from encounter, ΔM = ΔV propellant

Table 15. ΔV, ΔM Profile: Trajectory with Error Corrections at Maneuvers (Case B)

TCM	Time dd mmm yy	Time (dFE)	ΔV (km/s)	ΔM (kg)
1	21 Feb 99	-1776	0.000E+00	0.000
2	10 Mar 00	-1393	1.612E-01	28.584
3	13 Apr 00	-1359	4.036E-04	0.069
4	16 Nov 00	-1142	5.017E-03	0.854
5	05 Jan 01	-1092	4.668E-04	0.079
6	14 Feb 01	-1052	2.093E-03	0.355
7	30 Nov 01	-763	3.365E-03	0.569
8	14 Jul 03	-172	6.733E-02	11.178
9	23 Jul 03	-163	1.301E-04	0.021
10	03 Dec 03	-30	6.782E-03	1.105
11	23 Dec 03	-10	5.464E-04	0.089
12	31 Dec 03	-2	5.464E-04	0.089
13	02 Jan 04	-0.25	2.081E-03	0.338
14	01 Feb 04	+30	5.133E-03	0.832
15	01 Oct 04	+273	1.837E-03	0.297
16	16 Nov 05	+684	1.156E-02	1.858
17	02 Jan 06	+731	1.844E-03	0.295
18	14 Jan 06	+743	3.728E-04	0.057
		Total:	2.707E-01	46.581

Table 16. ΔV, ΔM Profile: Optimal Trajectory with ACS Model (Case C)

TCM	Time dd mmm yy	Time (dFE)	ΔV (km/s)	ΔM (kg)
2	10 Mar 00	-1393	1.611E-01	28.569
7	30 Nov 01	-763	7.054E-04	0.116
8	14 Jul 03	-172	6.468E-02	10.795
14	01 Feb 04	+30	1.414E-03	0.231
		Total:	2.279E-01	39.711

Table 17. ΔV Mass Consumption

Mass Quantity (kg)	Case A	Case B	Case C
End of mission spacecraft	358.096	345.331	352.253
ΔV+ACS propellant	39.904	52.669	45.747
ACS propellant	0.000	6.088	6.036

Using typical ACS perturbation magnitudes of $4x10^{-11}$ to $10x10^{-11}$ km/s^2, in one day (t=86,400 s), the position and velocity errors due to ACS activity are bounded at 0.15 to 0.38 km, and 3.5 to 8.8 mm/s, respectively.

ACS Perturbation Discussion

Tables 14 through 17 show that the real deterministic ΔV expenditure, when the trajectory design includes ACS activity modeling is 228 m/s. The less involved approach (Case B) would have cost the mission 271 m/s. The conclusion is that the labor of ACS force simulation and reoptimization saved the mission 43 m/s (19%) in ΔV budget.

It is interesting to note that the ΔV requirement indicated for case C is similar to the simple and inaccurate case A. This is not to say that the two cases have similar ΔV history. They are similar in cumulative ΔV but differ in individual magnitude and direction. The cumulative (scalar sums of magnitude) ΔV resulting from the 6.036 kg ACS burns is about 16.3 m/s. Comparing the Case A and Case C in total ΔV, one arrives at the conclusion that, by biasing the trajectory to compensate for the presence of ACS ΔV's no extra ΔV (compared to the case of no ACS) is incurred. However, if one did not take the trouble to compensate for the ACS burns in the planning stage, one would be required to pay more than twice the ACS imparted ΔV during the flight.

The impact of ACS perturbations on navigation deliveries is important in two cases: Wild-2 encounter and Earth return. Navigation delivery errors at encounter are expected to be on the order of 6 km in position $(1\text{-}\sigma)$[4]. Thus, one concludes that the contribution of ACS perturbations is insignificant. On the other hand, Earth return delivery errors are expected to be on the order of 0.38 km in position $(1\text{-}\sigma)$. In this case, the contribution of ACS perturbations is comparable to the navigation delivery and should not be ignored.

Summary

Simulation of unbalanced ACS activity during the STARDUST trajectory design has significant benefits. Though cumbersome, the modeling effort allows biasing of the trajectory to compensate for the presence of ACS activity and precludes unexpected, post-launch, ΔV costs. The modeling work also allows identification of key mission events where navigation must account for the effect of the ACS activity to ensure successful delivery of the spacecraft and sample return capsule.

Acknowledgments

The authors wish to acknowledge the STARDUST Attitude Control Team at Lockheed Martin Astronautics, especially Jason Wynn and Eric Lander, and the Mission Analysis Software programmers at the Jet Propulsion Laboratory, especially Edward Rinderle and Larry Bright. Without their contributions, the development of these ACS models and their integration into JPL's trajectory optimization software would have been extremely difficult.

References

1. Yen, C., Hirst, E., "Stardust Mission Design", AAS 97-707, AAS/AIAA Astrodynamics Specialist Conference, Sun Valley, Idaho, August 4-7, 1997.
2. Wynn, J., "Stardust Cruise ΔV Approximation", SD-TM-053, June 30, 1997.
3. Wynn, J. "Stardust Communications Slew Description", SD-TM-206, February 20, 1998.
4. Stardust Navigation Plan, SD-76000-100, pp. 14, June 14, 1998.